Towards a link between the energetic heterogeneities of the edge faces of smectites and their stability in a context of metallic corrosion

Murielle Perronnet, Frédéric Villiéras, Michel Jullien, Angelina Razafitianamaharavo, Joël Raynal, Dominique Bonnin

Towards a link between the energetic heterogeneities of the edge faces of smectites and their stability in the context of metallic corrosion

Revision 1 - 12/6/2006

Murielle Perronnet [1, 2*+], Frédéric Villiéras [1*], Michel Jullien [2], Angelina Razafitianamaharavo [1], Joël Raynal [2], Dominique Bonnin [3]

[1] Laboratoire Environnement et Minéralurgie, UMR 7569 Nancy-Université - CNRS, Ecole Nationale Supérieure de Géologie, BP 40, 54501 Vandoeuvre les Nancy Cedex, France

[2] Laboratoire de Modélisation des Transferts dans l'Environnement, Commissariat à l'Energie Atomique, Centre de Cadarache, Bâtiment 307, 13108 Saint Paul les Durance, France

[3] Laboratoire de Physique Quantique, Ecole Nationale Supérieure de Physique Chimie Industrielle de Paris, 10 rue Vauquelin, 75231 Paris Cedex 05, France

* Corresponding authors:

murielle.c.perronnet@nasa.gov

Frederic.Villieras@ensg.inpl-nancy.fr

[+] Present address: Lyndon B. NASA Johnson Space Center, KT, 2101 Nasa Road One, Building 31 Room 236, Houston, TX 77058-3696, USA

1. ABSTRACT

In the context of the potential confinement of high-level radioactive wastes (HLW) within the clay Engineered Barrier System (EBS) in deep geological formations, the evolution of the retention properties of smectite when interacting with Fe(0) needs to be assessed. If some potential natural analogues describing iron-clay reactivity are easily found, metallic iron-clay interactions are poorly described in studies regarding the Earth. Therefore experimental investigations are needed. Several parameters influence Fe(0)-clay interactions, such as temperature, the interlayer composition of swelling clays, and the presence of octahedral Fe^{3+}… From a geometrical point of view, it is thought that clay destabilization is mainly controlled by phenomena starting at the edge faces of the particles.

In the present work, the rates of the smectite-Fe(0) reaction at 80°C was assessed by XRD, Mössbauer and CEC analyses for three smectites. The investigations show marked differences in the degree of stability, which can not be explained by the crystal-chemistry rules established in previous studies. Therefore, the Fe(0)-smectite interactions were studied in view of textural and energetic surface quantitative analyses. The studied smectites have equivalent nitrogen BET specific surface areas, equivalent argon edge surface areas and slightly different basal surface areas. This similarity in particle shape indicates that the edge surface area can not be accounted for when explaining the observed differences in reactivity. However, a correlation is obtained between smectite reactivity and the energetic heterogeneity of its edge faces. This is interpreted in terms of a multiplication of the number of sites on the edge faces, where the electron transfer between Fe(0) and the smectite structure can occur.

2. INTRODUCTION

Iron-clay reactions are of great importance in soils and in sedimentary and diagenetic processes. In soils, the evolution of clay minerals is mainly controlled by oxidation-reduction reactions. Kaolinite is very reactive in media under varying redox conditions, but Fe-rich TOT clay minerals are even more reactive, and great changes in their properties may occur (e.g. Favre et al. 2002). Low temperature, iron-rich, clayey environments are also described in sedimentary verdine facies (Bailey 1988; Odin 1988; Odin 1990), in diagenetic oolitic ironstones (Bhattacharyya 1983; Bhattacharyya 1986) and in sandstones (Hornibrook and Longstaffe 1996; Aagaard et al. 2000; Hillier and Velde 1992; Hillier 1994). In these natural systems, iron is present as iron oxides and/ or hydroxides (e.g. Odin 1988; Buatier et al. 1989; Walker and Thompson 1990; Hornibrook and Longstaffe 1996), although metallic iron, Fe(0), has only been identified in contact with clay in extraterrestrial materials, such as CM carbonaceous chondrites. In this case, when heating of the asteroid induces fusion of accreted ice, cronstedtite, a Fe-rich 7Å mineral, is formed by interaction between olivine and FeNi metal (Zolensky and McSween 1988; Brearley 1997; Zega and Buseck. 2003). However, recently the clay-Fe(0) interactions in terrestrial environments are in question. Indeed, clay minerals may be used to confine the metallic canisters of high-level radioactive wastes (HLW) in deep geological formations.

Because of the lack of information concerning the Fe(0)-clay interactions on Earth, experiments have to be carried out to test clay stability when in contact with metallic iron for different temperatures, saturation states and redox conditions.

In a previous study, Perronnet (2004) demonstrated that it is mostly the smectite fraction of the clay material which reacts with Fe(0). At temperatures up to 200°C (Habert, 2000; Lantenois, 2003; Perronnet, 2004), smectite minerals are altered into Si-Al-Fe gels which mature into Fe-rich 7 Å minerals. At 300°C, Guillaume (2002) and Guillaume et al. (2003) indicated that smectites are converted into Fe-rich 14 Å chlorites. Lantenois (2003) and Lantenois et al. (2005) carried out experiments with different smectites in order to evidence the cristallo-chemical features which influence smectite/Fe(0) interactions. Results are described by the Lantenois' rules: at 80°C, the oxidation of metallic iron by smectites i) occurs only for dioctahedral smectites and for pH>7; ii) is favored by the interlayer spacing (the proportion of altered smectite increases from K-, to Ca- to Na-saturated samples) and by the presence of Fe^{3+} in octahedral sheets even in very low amounts; iii) for a given Fe^{3+} content, the quantity of altered smectite is more important for beidellite (tetrahedral deficit) than for montmorillonite (octahedral deficit).

In the case of a composite clay material (FoCa7 bentonite), Perronnet (2004) indicated that in the presence of Fe(0) at 80°C, montmorillonites are more altered than beidellites. But the structural formulas of FoCa7 smectites (Gin et al., 2001) show that FoCa7 beidellites have a tetrahedral charge, a higher Ca^{2+} interlayer content and a higher Fe^{3+} octahedral content than FoCa7 montmorillonites. Therefore, the observations of Perronnet (2004) contradict Lantenois' rules and give evidence that other parameter(s) influence(s) the reaction rate of the smectite-Fe(0) interaction.

Other possible controlling parameters, which were not analyzed in Lantenois' work, are those describing the surface properties. Indeed, phyllosilicate surfaces have strong differential reactivity because of the extreme anisotropy of their structure (Cases et al., 1986; Bickmore et al., 2001), the irregular surface topography (e.g., kinks, edges and adatoms) and the

presence of defects (Metz et al., 2005). For example, concerning the alkaline dissolution of smectites (Sato et al. 2003), it has been confirmed that the reaction rate increases with pH and, using in-situ observations, that the dissolution is congruent and dominated by the reactivity of the edge faces of the mineral.

At present, two main techniques based on low pressure adsorption and Atomic Force Microscopy (AFM) are proposed to determine the geometrical heterogeneities of flat solids.

Low pressure adsorption techniques have been used for a long time to assess surface morphology and heterogeneity of phyllosilicates (Cases et al., 1986, 2000; Villiéras et al., 1992, 1997, 2002). Using low pressure adsorption microcalorimetry (Cases et al., 1986, 2000) or low pressure quasi-equilibrium adsorption manometry (Cases et al., 2000, Michot et al., 1990, 1994, Sayed-Hassan, 2005, 2006, Villiéras et al., 1992, 1997), it was established that the adsorption of argon on basal and edge faces of non polar phyllosilicates (talc, kaolinite) can be detected. Consistent basal and edge specific surface areas of charged, non-swelling and swelling lamellar minerals such as illite (Villiéras et al., 2002, Bardot, 1998, Bardot et al., 1998), lamellar silicas (Eypert-Blaison et al, 2002), saponites (Michot & Villiéras, 2002) and montmorillonite (Tournassat et al., 2003) were obtained from low pressure argon adsorption experiments.

Atomic Force Microscopy (AFM) is used to study crystal morphology and structure, microtopography, surface heterogeneities down to molecular scales and the distribution of surface areas (Blum, 1994; Nagy, 1994; Nagy and Blum, 1994; Hochella, 1995; Hochella et al., 1998; Brady et al., 1996; Nagy et al., 1999; Sutheimer et al., 1999; Bosbach et al., 2000; Bickmore et al., 2002; Tournassat et al., 2003; Metz et al., 2005). Atomic Force Microscopy presents the advantage of providing surface area data selectively for individual crystal faces and, when using this technique in-situ, it is possible to characterize the surfaces while the clay particles are exposed to an aqueous solution under defined conditions. The reactivity of

smectite surfaces has already been investigated using AFM techniques (e.g., Metz et al. 2005). It was shown that basal plane dissolution may contribute to phyllosilicate bulk dissolution rates (Blum, 1994; Huertas et al., 1999; Cama et al., 2002; Brandt et al., 2003; Ganor et al., 2003), but the dissolution process is dominated by the chemical attack on edge sites (Metz et al. 2005).

In a recent study, Tournassat et al (2003) showed that comparable morphological parameters of montmorillonite clay platelets can be obtained using AFM and low pressure argon adsorption. Particularly, it is useful for the determination of edge surface area and the perimeter to basal area ratio, which can be considered to be independent of the stacking conditions of the clay layers, as long as the stacking does not change the accessibility of argon to the lateral surfaces of the particles. Thus, each technique can be used depending on its availability and the required accuracy. Atomic force microscopes are more popular and accessible than low pressure argon adsorption setups. The main difficulty with AFM is the requirement of an important running time in order to analyze enough particles to get accurate statistical values (Sayed-Hassan et al., 2006). Moreover, sample preparation can be tricky (Bickmore et al., 1999; Metz et al., 2005). Low-pressure argon adsorption seems more advantageous to derive mean values for samples having broad particle size distributions because of the huge amount of particles taken into account in the adsorption system (Sayed Hassan et al., 2006).

In this context, our objective is to analyze the possible links between the reaction rate of smectite/Fe(0) and the geometric and energetic characteristics of the basal and edge surfaces of different dioctahedral smectites. The reactions between three different smectites and Fe(0) were studied by short-term tests (3 months) at 80°C and the initial geometric and energetic

properties of these smectites were analyzed by classical nitrogen adsorption/desorption at 77 K and low pressure argon adsorption at 77 K.

150

151 # 3. MATERIALS AND METHODS

152

153 ## 3.1. Reagents

154

155 *3.1.1. Smectites*

156

157 Lantenois' rules (Introduction) indicate that smectites react with Fe(0) if they are
158 dioctahedral. The reaction rate is influenced by the octahedral Fe^{3+} content as well as the
159 interlayer spacing. For these reasons, three dioctahedral smectites having varied Fe^{3+} content
160 were selected. They were also chosen because of the low content (in accessory minerals) of
161 the bentonite from which they are extracted, and because they have equivalent surface
162 characteristics (specific surface area, edge surface area)**.** Montmorillonite OrduArtikli was
163 extracted in the Ordu area of the Eastern Pontides in Turkey and was provided by the Société
164 Française des Bentonites et Dérivés (SFBD). Beidellite "Nontronite" is a Fe^{3+}-rich beidellite
165 which is abusively called nontronite. It was provided by Ward's. Montmorillonite Prassa was
166 extracted in the quarry of the Kimolos Islands in Greece and was provided by the SFBD.
167 The argillaceous nodules were separated from the bulk bentonite for OrduArtikli and Prassa.
168 Then, the smectite fraction of the 3 samples was extracted by successive sieving-separations
169 to remove coarse particles. The structural formula of OrduArtikli
170 $(Si_{3.92}Al_{0.08})(Al_{1.29}Fe^{3+}_{0.14}Fe^{2+}_{0.04}Mg_{0.53})Ca_{0.2}Na_{0.12}Mg_{0.06}K_{0.01}$ (Habert et al., 2006)
171 Nontronite $(Si_{3.64}Al_{0.36})(Al_{1.0}Fe^{3+}_{0.93})Ca_{0.29}$, and Prassa
172 $(Si_{3.92}Al_{0.08})(Al_{1.54}Fe^{3+}_{0.10}Mg_{0.44})Ca_{0.08}Na_{0.06}K_{0.05}$ (Christidis, 1998) per $O_{10}(OH)_2$ were
173 established by EDS-TEM microchemical analyses.

The purified smectites were Ca-exchanged in order to avoid the influence of interlayer cations during the smectite-Fe(0) test.

3.1.2. Evian natural mineral water

Evian mineral water (France) was chosen because its chemical composition is stable and similar to the pore water chemistry of argillaceous or calcareous formations. It is mainly bicarbonate and magnesia rich water (Table 1).

3.1.3. Metallic iron

Metallic powder was used to simulate the iron fluxes released by the metallic part of a radioactive waste disposal. Metallic iron was purchased from Merck and is a 99.9778 wt% pure Fe(0) powder containing N, Cl, S, Pb, Cu, Mn, Zn and As as trace elements. Its small diameter, 10 μm, insures high reactive surface area and, therefore, enhances the reaction-rate.

3.2. Smectite purification

Samples used in this study were previously purified in order to control chemical and physical properties of the reacting clay. The purification procedure (Kohler 2001) is based on powder dispersion in purified water for 24 hours (100 g clay, 1 L water). Purified water was then added drop by drop to the agitated clay-suspension and wet sieved using a set of vibrating sieves (200 μm and 20 μm).

197 The <20 μm clay fraction was then diluted in purified water and centrifuged (10000 rounds
198 per minute) for 30 minutes. The solid was freeze-dried and hand-ground into a mortar.
199 To control interlayer composition, purified smectites were dispersed in deionized water with
200 clay content lower than 50 $g.L^{-1}$ and exposed to 0.1 M $CaCl_2$ (for smectites used in the tests
201 with Fe(0)) or 1 M NaCl (for smectites used in gas adsorption analyses), as it was
202 demonstrated that the exchangeable cations used should be lithium or sodium, to derive an
203 accurate argon specific surface area and aspect ratio (Bardot, 1998; Bardot et al., 1998;
204 Villiéras et al., 2002; Sayed-Hassan et al. 2005). The solutions were left in dialysis
205 membranes for a duration of 24 hours. Three exchanges followed using several washings in
206 purified water, in order to remove excess ions. After the last wash step, the clay fraction was
207 extracted from the dialysis pocket, centrifuged (10000 rounds per minute) for 30 minutes,
208 freeze-dried, gently ground into a mortar and homogenized.
209 As observed by Christidis (1998), the purified Prassa sample contains opal-CT as an
210 accessory contaminant. From a mineralogical point of view, the comparison between the
211 measured CEC (74 meq/100g) and the CEC calculated from half the unit cell (75 meq/100g)
212 suggests that the amount of opal-CT is around 2% in the purified sample. Opal is known to
213 dissolve in slightly to moderately alkaline solutions. Its specific surface area ranges between
214 7 and 15 m^2/g (Bustillo et al. 1993). Taking into account the low amount of this mineral in
215 the studied sample, it can be assumed that its influence is negligible on measured specific
216 surface areas.
217
218 **3.3. Experimental media**
219
220 To perform Fe(0)/clay reaction tests, purified Ca-exchanged smectites, metallic iron and
221 Evian water were mixed together in 50 mL polysulfone Nalgene test tubes. Fe(0)/Clay mass

ratios (I/C) of 0 and 1/3 and clay/solution mass ratios of 1/16.7 were used. The duration of the experiment was fixed to 3 months. The experimental temperature of 80 °C was obtained by heating the test tubes in a thermostatic oven. After the time was complete, samples were quenched and centrifuged at 7300 rpm for 150 minutes. Sealed test tubes were then introduced into a glove box in order to measure the pH of the supernatant and to separate solutions from solid phases. The solid phases were then freeze-dried, gently ground into a mortar, homogenized and stored in hermetically closed and vacuumed boxes.

3.4. Analytical methods

3.4.1. pH measurements

The pH measurements of the supernatant were carried out at room temperature using a Denver Instrument 215 pH-meter.

3.4.2. Cation Exchange Capacity

The Cation Exchange Capacity (CEC) of the samples were measured using the Cu-ethylenediamine (Cu-En_2) method (Mantin, 1969), suitable for solutions with pH > 6. Thirty milliliters of Cu-En_2 and 0.5 g of clay were mixed and shaken in a Turbula for two hours. The mixture was centrifuged at 7300 rpm for 30 minutes and the extracted solution was filtered at 0.22 µm. The residual Cu-En_2 concentration was then determined by measuring the absorbance at 548 nm with a Beckman DU-7000 spectrophotometer.

3.4.3. ^{57}Fe Mössbauer Spectroscopy

^{57}Fe Mössbauer spectroscopy was used to estimate the respective amounts of iron in the clay structures as well as in oxyhydroxides and magnetic phases. This method also gives the respective amounts and coordination nuber of Fe^{2+} and Fe^{3+} in the clay fraction.

One millimeter thick samples were obtained from pellets of homogenized powder, coated with Epoxy resin, dried under a vacuum box at 25 °C and polished.

Spectra were recorded on a Mössbauer spectrometer with a 15 mCi source of ^{57}Co in rhodium. They were taken in constant triangular acceleration mode in 512 channels. The spectrometer was calibrated at room temperature (RT) with a 25 μm foil of α-Fe, the isomer shifts are given with respect to α-Fe. A limited number of components (sextet and doublet) were used to fit the spectra using the MOSS program written by Bonnin (ESPCI Paris). In this program, magnetic hyperfine-field distributions of the components, which are common in soil Fe-oxides, are treated according to the model developed by Bocquet et al. (1992). Spectra obtained at low (15 K) and room temperatures differed only in the smaller distribution width of the magnetic lines of ternary oxides in the low temperature spectra. As this distribution width had no influence on our analysis of ternary oxide content, we obtained all reported spectra at room temperature.

3.4.4. X-Ray Diffraction

X-Ray Diffraction (XRD) patterns were recorded on non oriented samples to obtain qualitative mineral analysis of the samples. A D8 Bruker diffractometer (45 kV, 40 mA),

with CuKα radiation equipped with a graphite monochromator and a NaI scintillation detector was used.

3.4.5. Step by step nitrogen adsorption and high-resolution argon adsorption

Nitrogen adsorption–desorption isotherms at 77 K were recorded on a step-by-step automatic home-built setup described in Neaman et al. (2003) and Marrocchi et al. (2005). Pressures were measured using 0–1000 Pa and 0–100,000 Pa Baratron-type pressure sensors provided by Edwards. The nitrogen saturation pressure was recorded in situ using an independent 0-100,000 Pa Baratron-type pressure sensor provided by Edwards.

Specific surfaces areas (SSA) were determined from adsorption data by applying the Brunauer–Emmet–Teller (BET) equation (Brunauer et al., 1938) and using 16.3 $Å^2$ for the cross-sectional area of nitrogen (Gregg and Sing, 1982) In the present study, the error in the determination of the SSA was estimated as ±4 m^2/g. Micropore volumes and nonmicroporous surface areas were obtained using the t-plot method proposed by de Boer et al. (1966). Pore size distributions and mesopore volumes were calculated according to the BJH method (Barrett et al., 1951; Olivier, 1996).

Approximately 250 mg of purified Na-exchanged smectites were out gassed overnight at 110°C and under a residual pressure of 0.01 Pa. Nitrogen N55 (purity >99.9995%) used for experiments was provided by Alphagaz (France).

The experimental procedure for high-resolution and low-pressure argon adsorption has been discussed by Rouquerol et al. (1988), Michot et al. (1990) and Marrocchi et al. (2005). The quasi-equilibrium manometric technique proposed by Grillet et al. (1977) and Rouquerol et al. (1988) was used to enhance the resolution of the adsorption isotherms in the low-pressure range, when the first layer of gas is adsorbed on the surface. Using pressure sensors that work

294 at low pressures, this method allows the study of surface heterogeneity of solids under
295 appropriate conditions. In the case of phyllosilicates, it has been demonstrated that such
296 adsorption experiments, coupled with a careful analysis of experimental adsorption
297 isotherms, enable a derivation of a shape factor, i.e., lateral and basal surface areas (Bardot et
298 al., 1998; Cases et al., 1986, 2000; Michot et al., 1994, 2002; Sayed-Hassan et al., 2005,
299 2006, Villiéras et al., 1992, 1997a, 1997b, 2002).
300 The quasi-equilibrium technique is based on adsorbate introduction with a slow, constant and
301 continuous flow rate through a micro leak (Rouquerol et al., 1988, Michot et al., 1990). The
302 flow rate was kept constant, at least up to the BET domain, and was controlled by the
303 pressure imposed before the leak. If the introduction rate is low enough, measured pressures
304 can be considered quasi-equilibrium pressures. Then, from the recording of quasi-equilibrium
305 pressures (in the range of 10^{-3} to 3 10^{4} Pa) as a function of time, the adsorption isotherm was
306 derived. The set-up used has been described in Villiéras et al. (1997b) and Marrocchi et al.
307 (2005). For argon adsorption, 77 K sample temperature is insured by a dynamic and accurate
308 constant level of liquid nitrogen which was itself controlled by a home-made electronic
309 device. Three high accuracy MKS differential pressure transducers were used for pressure
310 measurements: (1) 0-1.3 Pa, (2) 0-1.3 10^{2} Pa and (3) 0-1.3 10^{5} Pa (698 type Baratron pressure
311 transducers). The minimal sensitivities were 1.3 10^{-4}, 1.3 10^{-2} and 1.3 Pa for gauges (1) to (3)
312 respectively. Pressure accuracy was 0.05% of read pressure. A dynamic pressure, lower than
313 10^{-3} Pa, was ensured on the reference side by the use of a turbomolecular vacuum pump. The
314 frequency of the pressure recording was adjusted after each measurement to record 100-200
315 experimental points per unit log of relative pressure. Thus, 2000 to 3000 experimental points
316 were collected per experiment for relative pressure lower than 0.15 (Villiéras et al. 1992,
317 1997b).

318 The experimental information was analyzed using the Derivative Isotherm Summation (DIS)
319 procedure designed by Villiéras et al. (1992, 1997a, 1997b), to examine the surface energetic
320 heterogeneity of the samples. Due to the large number of experimental data points acquired
321 by the quasi-equilibrium technique, the experimental derivative of the adsorbed quantity as a
322 function of the logarithm of relative pressure could be calculated accurately. In the present
323 case, samples were considered as not microporous for argon (see results section) and
324 multilayer adsorption could be mathematically removed from experimental adsorption
325 isotherms. The derivatives then corresponded to the first layer free energy adsorption
326 distribution and could be regarded as fingerprints of interactions between given solid/probe
327 couples.
328 The total derivative adsorption isotherm on a heterogeneous surface was modeled by
329 considering two scales of heterogeneity: in the case of crystalline minerals, the surface can be
330 divided into i different crystal faces (patchwise distribution), each face having its own
331 heterogeneity continuously distributed around a mean value (random distribution). The
332 adsorption isotherm on such a heterogeneous surface can be written as:

333 $$\theta t = \sum_i X_i \theta_{it} = \sum_i X_i \int_{\Omega} \theta_i(\varepsilon).\chi_i(\varepsilon).d\varepsilon$$

334 where θ is the total adsorption isotherm, θ_{it} the adsorption isotherms on the different energetic
335 domains of the surface, X_i is its contribution to θ_{it}, ε is the adsorption energy, Ω is the
336 physical domain of ε, $\theta_i(\varepsilon)$ a "local" theoretical adsorption isotherm and $\chi_i(\varepsilon)$ is the dispersion
337 of ε on the i^{th} domain. The experimental curve can then be fitted with theoretical local
338 isotherms derived from the Langmuir (with Bragg-William-Tempkin improvement to take
339 into account lateral interaction), BET (with Hill improvement to take into account lateral
340 interactions) and Dubinin-Astakhov formalisms (Villiéras et al., 1992, 1997a, 1997b).
341 In the present work, experimental derivatives were modeled after mathematical elimination of
342 multilayer adsorption contribution in the low energy region (right hand side of the curves)

(Villiéras et al., 1997a; Manleev et al., 2002). DIS fitting procedure was then applied to the first layer free energy adsorption distribution using the Bragg-William-Tempkin model as a local adsorption isotherm (Villiéras et al., 1992, 1997a, 1997b). Each local isotherm is characterized by three parameters. The first one is the peak position, $\ln(P/P_0)$, proportional to the free adsorption energy ΔG ($\Delta G = - RT.\ln(P/P_0)$), linked to C_{BET} constant, i.e. the normal interaction between the surface and an adsorbed molecule. The second one is the lateral interactions, ω, between two neighboring adsorbed molecules. Lateral interactions are easily detected through the shapes (half-height width) of the local derived isotherm. In fact, the intensity of lateral interactions must be considered as a best-fit parameter, disclosing further information about the heterogeneity of the considered adsorption domain (Bardot, 1998, Bersillon et al., 2001; Mamleev et al., 2002; Villiéras et al., 1997b): generally, ω ranges between 2.5 and 0 for argon, and lower values (even negative values) are obtained when the spreading (variance) of the adsorption energy distribution increases. The last consideration is the monolayer capacity, V_m, of the local isotherm, derived from the comparison between the experimental height of the peak and the theoretical height of the local model. Monolayer capacities can be converted to surface areas by taking into account the cross-sectional area of adsorbed argon, 13.8 A² (McClellan and Harnsberger, 1967).

In our study, about 0.6 g of purified Na-exchanged smectites were out gassed at 0.001 Pa at a temperature of 120°C. Argon N56 (purity>99.9996) was supplied by Alphagaz (France).

4. RESULTS

4.1. Smectite reactivity in the context of metallic corrosion

4.1.1. pH measurements

pH was systematically measured to control the basic character of Fe(0)/Clay interactions. In each case, the pH was over 7 (Table 2).

When comparing the pH of the solution with I/C=1/3 and without iron (I/C=0), it was observed that the presence of Fe(0) had no effect on pH for the test using OrduArtikli, whereas increases in pH of 0.7 and 2.6 were recorded for the tests with Nontronite and Prassa samples respectively.

4.1.2. Cation Exchange Capacity

The Cation Exchange Capacity (CEC) of each sample was measured before and after the reaction (Figure 1 and Figure 2) to verify the stability of smectite during reaction tests. Due to the precision of CEC measurements, only variations greater than 10 % were considered significant.

The CEC values for unreacted samples decreased with respect to Fe(0) supply, in agreement with the dilution effect caused by the addition of metallic iron to the experimental suspension.

When heating at 80°C for 3 months without iron (Figure 1), the CEC variations are -10 %, -1 % and +22 % for Orduartikli, Nontronite and Prassa samples respectively. These variations were only significant for the Prassa sample.

With Fe(0) in the reaction mixture (Figure 2), the CEC variations are -4 %, +16 % and -37 % for Orduartikli, Nontronite and Prassa samples, respectively. Only the CEC variations for Nontronite and Prassa samples could be considered significant.

In conclusion, Fe(0) supply influences the CEC of Nontronite and Prassa clays, but not that of OrduArtikli clay.

4.1.3. ^{57}Fe Mössbauer spectroscopy

^{57}Fe Mössbauer spectroscopy was used to quantitatively determine the modifications in the distribution of iron species. Since there is no modification of the XRD (see next §) and CEC value after interaction between OrduArtikli and Fe(0), this sample is considered poorly reactive. Mössbauer spectra were only acquired for Nontronite and Prassa.

Before the reaction, the distributions of iron species in Nontronite-Fe(0) and in Prassa-Fe(0) mixtures were different (Figure 3 and Figure 4). Nontronite is a beidellite which contains Fe(III) whereas in the Prassa-Fe(0) mixture, the initial iron mainly comes from the Fe(0) supply. After reaction, the distribution of iron species was quite unchanged for Nontronite-Fe(0) mixture, unlike the Prassa-Fe(0) mixture (Figure 3 and Figure 4). There was only a slight consumption of Fe(0) for Nontronite (-3%, 1.79 10^{-2} mol before reaction and 1.74 10^{-2} mol after reaction), which is balanced by the formation of Fe(III) (+6%, 7.06 10^{-3} mol before reaction and 7.5 10^{-3} mol after reaction). For Prassa, the consumption of metallic iron is high (-64%, 1.79 10^{-2} mol before reaction and 6.45 10^{-3} mol after reaction.) and is balanced by the formation of Fe(III)-species (+2087%, 4.08 10^{-4} mol before reaction and 8.92 10^{-3} mol after reaction), Fe(II) species (+552%, 4.08 10^{-4} mol before reaction and 2.66 10^{-3} mol after reaction) and iron oxides (+278%, 2.51 10^{-4} mol before reaction and 9.49 10^{-4} mol after reaction). Magnetic spectra for these iron oxides correspond to a spinel structure, so these oxides may be magnetite. Mössbauer parameters for Fe(III) and Fe(II) are consistent with their presence in amorphous phases, such as gel phases, and/or phyllosilicate octahedral layers.

416

417 *4.1.4. X-Ray Diffraction (XRD)*

418

419 The X-Ray Diffraction was used to estimate the qualitative evolution of the smectite-Fe(0)
420 mixtures at 80°C over 3 months. In order to take into account the dilution effect created by
421 metallic iron supply, the X-Ray diffractograms of "I/C=1/3 mixtures" were compared before
422 and after reaction.
423 The X-Ray diffractogram of the reacted OrduArtikli-Fe(0) mixture did not show any
424 significant variation (Figure 5). The 15.14 Å, 4.48 Å, 3.04 Å, 2.57 Å and 1.50 Å peaks of
425 smectite did not change either in position or in intensity. The 2.02 Å peak of Fe(0) was also
426 unaffected.
427 The same conclusions were made for the Nontronite-Fe(0) mixture (Figure 6). On the XRD
428 pattern, the peaks of smectite are unchanged (14.93 Å, 4.53 Å, 3.03 Å, 2.58 Å and 1.51 Å).
429 Unlike OrduArtikli or Nontronite, the diffractogram of the reacted Prassa-Fe(0) mixture is
430 very different from the unreacted one (Figure 7). The peaks attributed to smectite (15.3 Å,
431 5.07 Å, 4.48 Å, 3.03 Å and 1.50 Å) are hardly visible. The intensity of the Fe(0) peak is also
432 much lower. In addition, new peaks can be seen at 7.22 Å, 7.13 Å, 3.56 Å, 2.96 Å, 2.72 Å
433 and 2.53 Å. The 7.13 Å, 3.56 Å and 2.53 Å peaks may be related to the formation of Fe-rich
434 7 Å minerals such as berthierine (JCPDS 31-618). As observed by Lantenois et al. (2005),
435 2.96 Å, 2.53 Å and 1.48 Å peaks are assigned to the formation of magnetite (JCPDS 19-629).
436 On the XRD spectra (peaks at 4.07 Å and 2.48 Å), opal-CT is visibly present in the Prassa-
437 Fe(0) unreacted mixture, whereas it is not visible in the reacted mixture. It is known that
438 silica is soluble in water from pH=9. When Prassa is altered without Fe(0) at 80°C for 3
439 months, the pH equals 8 and opal-CT remains present in the reacted mixture (Perronnet,

2004). The same result was obtained for I/C=1/20 (pH=8) and I/C=1/10 (pH=8) (Perronnet, 2004), whereas opal-CT disappeared from I/C=1/3 when the pH reached 10.6.

4.2. Geometric and energetic surface properties

4.2.1. Nitrogen adsorption/desorption at 77 K

Nitrogen adsorption/desorption experiments were carried out to obtain main information on the textural properties of the studied samples: specific surface areas and pore size distribution. Adsorption/desorption curves are shown in Figure 8. First of all, it should be pointed out that adsorption/desorption isotherms present the classical features observed for swelling clays (Michot & Villiéras, 2002, Neaman et al., 2003, Marrocchi et al., 2005) with both microporosity and mesoporosity. In the low pressure region (<0.4), corresponding to the filling of micropores and the completion of the first monolayer on external particle faces, adsorption isotherms are superimposed, showing that the total specific surface areas of the three samples are within the same range. This is confirmed when the different numerical analyses are applied to experimental data (Table 3). Indeed, BET, t-plot and mesoporosity calculations yield specific surface areas ranging between 101 and 115 m^2/g. BET specific surface area is slightly lower than those derived from t-plot and mesoporosity calculations, which is in agreement with the fact that the samples appear slightly microporous. Microporosity is less important for Prassa than for Nontronite and Orduartikli and external surface area (without micropores) of particles increases from Orduartikli to Nontronite and Prassa. For the three samples, microporosity is not quantitatively important (compared to zeoliths or activated carbons, for instance) and errors on the determination of micropore volumes should be considered as important for such systems (+/- 20%). In addition, it should

465 be pointed out that the assessment of microporosity for charged clay minerals is rather tricky,
466 as it was demonstrated that specific interactions between nitrogen and surface cations (Bardot
467 et al., 1998, Michot and Villiéras, 2002) can occur in such a way that the total amount of
468 adsorbed nitrogen molecules on the surface would appear higher than the amount required for
469 monolayer completion (Michot et Villiéras, 2002). The corresponding additional adsorbed
470 amount would be attributed to microporosity, as determined from t-plot procedure. This
471 phenomenon probably occurs in the present case, as nitrogen external surface areas derived
472 from the t-plot (+/- 20%) agree fairly with total argon surface areas derived from low
473 pressure adsorption experiments (see next section and S_{Ar} in Table 3), as pointed out by
474 Michot and Villiéras (2002) for different saponites.
475 In the high relative pressure region (> 0.45), corresponding to multilayer adsorption and the
476 filling of the mesoporosity, great differences are observed (Figure 8). Orduartikli appears
477 slightly mesoporous with a vertical closure of the hysteresis loop around 0.44 in P/Po, as is
478 generally observed for such materials and is typical of closed mesoporosity inside clay
479 aggregates (Neaman et al., 2003). The same features are observed for the Nontronite sample,
480 which is more mesoporous than Orduartikli. For Prassa, which is the most mesoporous
481 sample, the shape of the adsorption/desorption loop is different, suggesting a more open
482 intra-aggregate mesoporosity. The total calculated mesoporosities agree with present
483 observations (Table 3). Calculated pore size distributions (Figure 9) from the adsorption
484 branch and the desorption branch, which correspond to true Pore Size Distribution (PSD) and
485 access PSD, respectively (Neaman et al., 2003), show that pore access corresponds mainly to
486 pores smaller than 2.5 nm. This is not seen in the Prassa sample, which presents an additional
487 access size around 3.8 nm. The differences in mesoporosity observed for the studied samples
488 can not yet be fully explained. Indeed, particle arrangement and pore size distribution of
489 swelling clay minerals differ considerably in the same sample, depending on dehydration

conditions, apparent density, exchangeable cations, etc. (Neaman et al., 2003, Michot and Villiéras, 2006, Bihannic, 1998). In the case of the Prassa sample, PSD may also be influenced by the presence of small opal-CT particles in clay aggregates. Mesopore size distribution, however, is not considered a key parameter for the present study, as particles and aggregate organizations will be different in suspension, i.e. under smectite/Fe(0) interaction conditions.

4.2.2. Low pressure argon adsorption at 77 K

Low pressure argon adsorption at 77 K was carried out in order to derive information on the surfaces of smectite particles and to analyze it from the point of view of variability in geometric (lamellarity) and energetic (surface chemistry) characteristics. The experimental curves obtained in the region corresponding to the adsorption of the first monolayer (P/Po=0 to 0.175, BET region) are displayed in Figure 10 as a function of the logarithm of the relative pressure. On this figure, it can be observed that the features are similar and adsorbed amounts are within the same range in all samples, as previously observed with nitrogen.

The present curves were further analyzed using the derivative adsorption isotherm instead of the adsorption isotherms, as these curves are much more sensitive to the influence of surface heterogeneities. The obtained derivative curves are displayed in Figure 11 along with their fit, using the DIS procedure designed by Villiéras et al. (1992, 1997). Adsorption energy distributions reveal the classical features observed for phyllosilicates, with a mean peak located around -5, corresponding to the adsorption on basal surfaces, while the shoulder at higher energy, centered around -7, corresponds to the adsorption on edge faces.

514 Using the DIS procedure and the Brag-William-Temkin equation, the three derivatives are
515 modeled with 5 local isotherms. As is usually obtained with argon, the 3 high energy peaks
516 (N° 1 to 3 in Table 4) can be assigned to the adsorption on edge faces, and the two low
517 energy peaks (N° 4 and 5 in Table 4) to the adsorption on basal faces.
518 It can be observed that the peak positions corresponding to basal faces (domain 4) are the
519 same for the 3 samples, around -4.5. In the same way, the corresponding lateral interaction
520 parameter ω can be considered as identical, 1.4 ± 0.1, for the three samples.
521 The situation is totally different for edge faces, as it can be observed that adsorption energies
522 for the less important domains 1 and 2 (inverse of peak positions) increases as follows:
523 Orduartikli < Nontronite < Prassa. From a chemical standpoint, these high energy adsorption
524 sites could be attributed to chemical variability or non-uniform morphology such as local
525 defects, corners or ridges of particle surfaces. The peak positions of domain 3, which
526 correspond to the most important part of the lateral surfaces, behave in the reverse order,
527 Prassa < Nontronite < Orduartikli. However, it is interesting to notice that the lateral
528 interaction parameter (ω/kT) also increases from Prassa to Nontronite and to Orduartikli
529 samples. This result indicates that i) edge surfaces of the Orduartikli sample can be
530 considered the most homogeneous (less variability in gas/surface site interactions), in
531 agreement with the fact that adsorption energies of domain 1 and 2 are the lowest of the
532 sample set; ii) edge surfaces of the Prassa sample can be considered to be the less
533 homogeneous, in agreement with the fact that adsorption energies of domain 1 and 2 are the
534 highest of the sample set; iii) homogeneity of the edge surfaces of nontronite is intermediary.
535 It can also be pointed out that peaks of domains 1 and 2 are often considered as residual and
536 their positions are generally not accurate. In the present case, the fact that the positions of
537 these peaks behave in the same way as the lateral interaction of the major peak (domain 3)
538 suggest that their evolutions within the samples are relevant.

From a quantitative point of view, the amount of high energy adsorption sites on edge faces (domain 1 and 2) correspond to 20, 26 and 19% of the total edge surface area for Orduartikli, Nontronite and Prassa, respectively, without correlation to the energy classifications discussed above. Total basal and lateral surface areas are reported on Table 5. Edge surface areas are in the same range for Orduartikli and Nontronite, while for Prassa, basal surface area is higher and edge surface area is lower than that of the two other samples. As proposed in Tournassat et al. (2003), mean characteristic length (l) and thickness (t) of the particles can be evaluated from basal and lateral surface areas by considering a simple square base:

$l = 4 / \rho \cdot Sl$ and $t = 2 / \rho \cdot Sb$

where ρ is the density (2.7) and *Sl* and *Sb*, the lateral and basal surface areas, respectively. The length of the particle increases from Orduartikli to Nontronite to Prassa (Table 5). This increase in length is probably at least partly responsible for the increase in mesoporosity as derived from nitrogen adsorption/desorption experiments. Taking into account the theoretical thickness of one dry smectite unit layer (taken to be equal to 9.5 Å), the average number of 2:1 layers per stack is around 15 for Orduartikli and Nontronite and 11 for Prassa.

5. DISCUSSION

The analyses of the reaction products show that smectites do not react equally with Fe(0). For OrduArtikli, the modifications in the pH, CEC and XRD diffractogram are negligible at the end of the "80°C-3 months-I/C=1/3" test. Concerning Nontronite, a slight increase in pH (+0.7), a slight consumption of Fe(0) (-3%) and formation of Fe(III) (+6%) and an increase in CEC (+16%) are observed while the intensity of the whole XRD spectrum is unchanged. On the contrary, for Prassa, the pH of the solution increases significantly (+2.6), the consumption of Fe(0) is drastic (-64%) and balanced by the formation of iron oxides and by the

564 incorporation of Fe(II) and Fe(III) in gel phases or in clay octahedral sheets. The decrease in
565 CEC (-37%) is important and on the XRD pattern, the signal of smectite is hardly
566 recognizable, while peaks for 7 Å clays and magnetite appear.
567 Lantenois et al. (2005) demonstrated that the percentage of altered smectites can either be
568 estimated by using XRD analyses in transmission geometry with an internal standard
569 (corundum) or by CEC measurements. These two methods gave the same results (fig 4a in
570 Lantenois et al. 2005) with the same precision (±10 %). In the present study, XRD and CEC
571 appear to be complementary techniques for sorting the samples with respect to their initial
572 reactivity. It is thus necessary to understand the meaning of the increase in CEC for
573 Nontronite and its decrease for Prassa. For this purpose, CEC results will first be analyzed in
574 the framework of bibliographic information on the destabilization mechanism of smectite
575 minerals. Finally, the reaction rates of the smectite-Fe(0) reactions will be put in parallel with
576 the geometric and energetic characteristics of the smectite surfaces.
577
578 **5.1. Destabilization mechanisms and relative reactivity of the studied smectites**
579
580 The reaction between smectites and Fe(0) can be described by three individual mechanisms:
581 1. The reduction of structural Fe^{3+} when smectite is in contact with Fe(0) or, more likely,
582 with Fe^{2+} resulting from the oxidation of Fe(0) (Lantenois et al., 2005, Wilson et al.,
583 2006). In reductive conditions, as is the case when clay minerals interact with Fe(0),
584 Fe^{3+} in smectites is reduced to Fe^{2+} with an increase of the layer charge, i.e. of the
585 CEC, which needs to be balanced by the uptake of H^+ or other cations in the interlayer
586 space (Stucki et al., 1984; Manceau et al., 2000; Favre et al., 2002,). The uptake in H^+
587 from solution causes the pH to increase.

2. The alkaline destabilization of smectite into Si-Al-Fe gels or disordered regions (Wilson et al., 2006). This mechanism occurs by edge dislocation, fragmentation in the [ab] plane, which makes the CEC increase, and by local loss of tetrahedral layers.
3. The incorporation of Fe^{2+}, derived from Fe(0) oxidation (Guillaume et al., 2004; Lantenois et al.; 2005, Wilson et al., 2006), into altered smectites (gel-like phases). These phases maturate into Fe-rich 7 or 14 Å non swelling minerals. That results in a decrease of the CEC of the reaction product (Guillaume et al, 2004; Perronnet, 2004; Lantenois et al., 2005; Wilson et al., 2006).

In the present study, it can be concluded from the stability of both the CEC values and the XRD pattern of OrduArtikli, that the reaction between this smectite and Fe(0) is not initiated. On the contrary, the significant decrease in CEC (-37 %) measured for Prassa samples in the presence of Fe(0), and the analysis of its run products by XRD and the formation of Fe-rich 7 Å clays, show that the reaction between smectite and Fe(0) is already advanced. The potential high reactivity of this sample is also suggested by its CEC increase (+22 %) at 80°C in the absence of iron supply, which may be attributed to some particle dissolution or/and fragmentation in high temperature water**.** In addition, it was observed that for intermediary I/C (1/20 and 1/10), the CEC of the reaction products increased in the same way while pH was stable at 8 (Perronnet 2004). When the supply in Fe(0) is important enough (I/C≥1/3), the oxidation of Fe(0) by smectites makes pH increase, in agreement with the smectitic corrosion mechanism proposed by Habert et al., 2006. It can also be noticed from XRD analysis that for I/Cs ranging from 0 to 1/10 opal did not react, showing that the dissolution of this phase may account for the increase in pH following the Fe(0)/smectite reaction.

In the case of Nontronite, the comparison of CEC results for the tests with and without Fe(0) at 80°C shows that, in both cases, the heating has no effect on this parameter. Therefore, the increase in CEC for the test in the presence of Fe(0) at 80°C is only a consequence of the

613 interaction of smectites with metal. This increase in CEC, without any significant structural
614 transformations observed in the XRD patterns, may correspond with the intake in cations
615 from the solution in order to balance the charge deficit due to the reduction of structural Fe^{3+}
616 by Fe(0) (stage 1). But, as the Mössbauer results indicate that this reduction did not happen
617 (Fe(III) +6%), fragmentation in the [ab] plane may be a more appropriate explanation for the
618 increase in CEC.
619
620 The destabilization rate of smectite when interacting with Fe(0) increases from OrduArtikli to
621 Nontronite and to Prassa samples. These smectites can be ranked with respect to the
622 tetrahedral layer charge (0.36 Nontronite > 0.08 OrduArtikli = 0.08 Prassa), the Ca^{2+}
623 interlayer content (0.29 Nontronite > 0.2 OrduArtikli > 0.08 Prassa), and the Fe^{3+} octahedral
624 content (0.93 Nontronite > 0.14 OrduArtikli > 0.10 Prassa) per $O_{10}(OH)_2$. According to
625 Lantenois' rules (2005), Nontronite should be more reactive than OrduArtikli, which also
626 should be more reactive than Prassa, which is in contradiction with our results. But,
627 Lantenois et al (2005) stressed that even if the reactivity of dioctahedral smectite is mainly
628 enhanced by increasing contents in octahedral Fe^{3+}, other parameters should be found in
629 order to fully understand the evolution of smectite-Fe(0) systems.
630
631 **5.2. Surface control of smectite reactivity towards Fe(0)**
632
633 As mentioned in the introduction, numerous studies demonstrated that transformations of
634 smectite minerals at the solid-liquid interface are mainly centripetal processes starting at the
635 edges of the layers. The determination of the mean textural features of the samples, based on
636 N_2 and Ar adsorption at 77K, allows us to compare particle shape, and particularly the
637 amounts of lateral surface area, with Fe(0)-smectite reactivity.

First of all, one can rapidly eliminate the dry particle shape as pertinent information; because, when immersed in water, smectites will expand with interlayer cation hydration, and the total number of clay layers per tactoïd is reduced. In addition, such parameters would lead to the conclusion that the finest particles in volume (Orduartikli) are the least reactive ones.

Edge surface areas are roughly equivalent for the three samples, but a fine analysis of the results shows that reaction rates increase when edge surface area decreases (Table 5). This is contradictory with the statement that the quantity of edge surfaces controls the reactivity. The definite differences in reactivity of the studied samples imply that edge surface area is not the main textural controlling parameter.

Basal surface area is equivalent for Orduartikli and Nontronite and is higher for Prassa. Considering the highest reactivity of the latter, it could indicate that basal faces of the clay layers control the iron-smectite reactivity, but such basal-control is not likely to be the most important mechanism, as it is contradictory to the admitted centripetal destabilization mechanism, and the total basal area should be roughly the same for the three samples in their hydrated state. Therefore something other than geometrical parameters should be found to explain the surface reactivity of smectites in the presence of Fe(0).

Other accessible parameters concern the energetic properties of argon/surface interactions. For the basal faces, the DIS peak positions and the apparent lateral interaction (ω) parameters of domain 4 (Table 4) are equivalent, and no significant conclusion can be drawn as to the influence of energetic surface properties of these faces on smectite reactivity. On the contrary, the edge faces show marked differences, particularly when looking at peak positions and apparent lateral interactions (ω). Indeed, these two parameters show that smectite reactivity increases with surface heterogeneity and the surface energy of their edge faces.

6. CONCLUSIONS

It seems that the destabilization rates of the smectite-Fe(0) systems can be at least partially explained by the energetic properties of the edge faces of the smectite. As stressed by Bickmore (1999) and Bickmore et al. (2001), the high reactivity of the edge surfaces is expected, because these surfaces are characterized by broken bonds and a well-known tendency to form inner-sphere complexes with protons and other cations (e.g., White and Zelazny, 1988; Zachara and McKinley, 1993; Charlet et al., 1993; Schlegel et al., 1999). Metz et al., (2005) stressed that the relationship between BET surface area and the reactive surface area is not trivial in minerals such as smectites, in which dissolution is controlled by chemical attack on the edge surfaces. These authors suggest using AFM measurements of the specific edge surface area as an alternative proxy for the reactive surface area of smectite. But they insist on the fact that their results do not prove that this proxy is proportional to reactive surface area. Indeed, it was observed that the dissolution kinetics of edge faces of smectites is much faster for broken edge faces than for euhedral faces (Bickmore 1999). The absence of a correlation with the edge surface area is confirmed by the fact that for our 3 smectites, the reaction rate for their alteration increases with respect to decreasing edge surface area. On the contrary, a positive correlation exists between the reaction rate for alteration and the variety in the energetics of gas adsorption onto the edge faces (energetic “heterogeneity of edge faces”). This variety illustrates the presence of i) crystallographic defects; ii) morphological heterogeneities, such as nanoroughness, or iii) chemical heterogeneities, such as clusters, substitutions and charge distributions as indicated by Bickmore (1999) and Bickmore et al. (2001). Such a variety of situations is obviously enhanced if lateral surfaces are broken edge faces rather than euhedral faces (Bickmore 1999).

688 Thus, the increase in the "energetic heterogeneity of edge faces" can be interpreted as an
689 increase in the probability for Fe(0) to find unstable sites on the smectite edges to transfer
690 electrons and initiate smectite destabilization. The rate controlling steps in the reaction seem
691 to be the reactions which occur on the sites of the edge faces. Both the fragmentation (with
692 and without Fe(0)) and the reduction, consecutive to electron transfer from Fe(0), of smectite
693 particles are enhanced when the heterogeneity of the edge faces is high. The ω parameter of
694 edge faces derived form argon adsorption can be considered as an exploration guide aiding
695 the prediction of the behavior of smectites in the context of alkaline dissolution and/or
696 metallic corrosion. It is also likely that the observed result reflects more the initiation
697 conditions for reactions, which are different than the final equilibrium state of the reacting
698 system.
699 The next step will be to confirm the validity of the present guide by determining the influence
700 of crystal-chemistry on ω parameter for a large set of samples, including non-swelling
701 minerals.

Acknowledgments. The authors would like to thank Jean-Claude Pétronin (LMTE) who made the CEC measurements and Philippe Lambert (LEM) who took part in the XRD study. Many thanks also to Claudine Pozo and Eric Kohler (LMTE) for their support of the experimental and analytical work. This work was carried out with the support of Catherine Santucci (LMTE) and Jacques Yvon (LEM), who welcomed Murielle Perronnet in their laboratories.

We thank Javier Huertas, Barry R. Bickmore and Ian C. Bourg for their high quality reviewing process. The authors do appreciate the suggestions of the reviewers, which served to improve the manuscript, as well as the hypotheses they offered and which were revealed to be pertinent to strengthen the reaction mechanisms. A great thanks also goes to the Associate Editor, Pr Sposito.

713

714 **7. REFERENCES**

715

716 Aagaard P., Jahren J. S., Harstad A. O., Nilsen O., Ramm, M. (2000) Formation of grain
717 coating chlorite in sandstones. Laboratory synthesized vs. natural occurrences. *Clay*
718 *Miner*. **35**, 261-269.

719 Bailey S. W. (1988) Odinite, a new dioctahedral-trioctahedral Fe^{3+}-rich 1:1 clay mineral.
720 *Clay Miner*. **23**, 237-247.

721 Bardot F. (1998) Les minéraux argileux et leur hétérogénéité superficielle: Influence de la
722 nature des cations compensateurs de l'illite sur les mécanismes d'adsorption de gaz. Ph.
723 D. thesis, Institut National Polytechnique de Lorraine, Nancy, discipline Géosciences.

724 Bardot F., Villiéras F., Michot L. J., François M., Gerard G., Cases J. M. (1998) High
725 resolution gas adsorption study on illites permuted with various cations: Assessment of
726 surface energetic properties. *J. Dispersion Sci. Technol.* **19**, 739-760.

727 Barrett E. P., Joyner L. G., Halenda P. H. (1951) The Determination of Pore Volume and
728 Area Distributions in Porous Substances. I: Computations from Nitrogen Isotherms. *J.*
729 *Am. Chem. Soc.*, **73**, 373-380.

730 Bhattacharrya D. P. (1983) Origin of berthierine in ironstones. *Clays Clay Miner*. **31**, 3, 173-
731 182.

732 Bhattacharrya D. P. (1986) Geochemistry of the phanerozoic oolitic ironstones-genetic
733 implication. *Am. Assoc. Petr. Geo. B.* **70**, 5, 565.

734 Bersillon J. L., Villiéras F., Bardot F., Gorner T., Cases J. M. (2001) Use of the gaussian
735 distribution function as a tool to estimate continuous heterogeneity in adsorbing
736 systems. *J. Colloids Interface Sci,* **240**, 400-411.

737 Bickmore B. R. (1999) Atomic Force Microscopy study of clays mineral dissolution. Ph. D.
738 thesis, Virginia Polytechnic Institute, speciality Phylosophy in Geological Sciences,
739 117 pp.
740 Bickmore B. R., Bosbach D., Hochella M. F. Jr., Charlet L., Rufe E. (2001) In situ atomic
741 microscopy study of hectorite and nontronite dissolution: Implications for phyllosilicate
742 edge surface structures and dissolution mechanisms. *Am. Mineral.* **86**, 411-413.
743 Bickmore B. R., Nagy K. L., Sandlin P. E., Crater T. S. (2002) Quantifying surface area of
744 clays by atomic force microscopy. *Am. Mineral.* **87**, 780-783.
745 Blum A. E. (1994) Determination of illite/smectite particle morphology using scanning force
746 microscopy. In *Scanning probe microscopy of clay minerals* (eds. Nagy K. L., Blum A.
747 E.). Clay Minerals Society. pp. 172-203.
748 Bocquet, S., Pollard, R. J., Cashion, J. D. (1992). Dynamic magnetic phenomena in fine
749 particle goethite. *Phys. Rev. B: Condens. Matter*, **46**, 11657–11664.
750 Brady P. V., Cygan R. T., Nagy K. L. (1996) Molecular controls on kaolinite surface charge.
751 *J. Colloid Interface Sci.* **183**, 356-364.
752 Brandt F., Bosbach D., Krawczyk-Barsch E., Arnold T., Bernhard G. (2003) Chlorite
753 dissolution in the acid pH-range: A combined microscopic and macroscopic approach.
754 *Geochim. Cosmochim. Acta* **67**, 1451-1461.
755 Brearley A. J. (1997) Phyllosilicates in the matrix of the unique carbonaceous chondrite
756 Lewis Cliff 85332 and possible implications for the aqueous alteration of CI chondrites.
757 *Meteorit. Planet. Sci.* **32**, 377-388.
758 Brunauer S., Emmet P. H., and Teller E. (1938) Adsorption of gases in multimolecular layers.
759 *J. Am. Chem. Soc.* **60,** 309–319.
760 Buatier M., Honnorez J., Ehret G. (1989) Fe-Smectite-Glauconite transition in hydrothermal
761 green clays from the Galapagos spreading center. *Clays Clay Miner*. **37**, 6, 532-541.

762 Bustillo, M. A., Fort, R, Bustillo, M. (1993) Specific surface area and ultramicroporosity in
763 polymorphs of silica. *Eur. J. Mineral*. **5**, 1195-1204.
764 Cama J., Metz V., Ganor J. (2002) the effect of pH and temperature on kaolinite dissolution
765 rate under acidic conditions. *Geochim. Cosmochim. Acta* **66**, 3913-3926.
766 Cases J. M., Cunin P., Grillet Y., Poinsignon C., Yvon J. (1986) Methods of analyzing
767 morphology of kaolinites: Relations between crystallographic and morphological
768 properties. *Clay Miner.* **21**, 55-68.
769 Cases J. M., Villiéras F., Michot L. J. (2000) Les phénomènes d'adsorption, d'échange ou de
770 rétention à l'interface solide-solution aqueuse: 1. Connaissance des propriétés
771 structurales, texturales et superficielles des solides. *Compte Rendu de l'Académie des*
772 *Sciences*, Série II, **331**, 763-773.
773 Charlet L., Schindler P. W., Spadini L., Furrer G., Zysset M. (1993) Cation adsorption on
774 oxides and clays – the aluminium case. *Aquat. Sci.* **55**, 291-303.
775 Christidis G. E. (1998) Physical and chemical properties of some bentonite deposits of
776 Kimolos Island, Greece. *Appl. Clay Sci.* **13**, 79-98.
777 De Boer J. H., Lippens B. C., Linsen B. G., Brokhoff J. C. P., Van der Heuvel A., Osinga T.
778 J. (1966) The t-curve of multimolecular N2 adsorption. *J. Colloid Interf. Sci.* **23,** 577–
779 599.
780 Eypert-Blaison C., Villiéras F., Michot L. J., Pelletier M., Humbert B., Ghanbaja J., Yvon J.
781 (2002) Surface heterogeneity of kanemite, magadiite and kenyaite: a high resolution
782 gas adsorption study, *Clay Minerals* **37**, 531-542.
783 Eslinger E., Pevear D. (1988) *Clay minerals for petroleum geologists and engineers*. Society
784 of Economic Paleontologists and Mineralogists.

785 Favre F., Tessier D., Abdelmoula, M., Génin, J. M., Gates W. P., Boivin P. (2002) Iron
786 reduction and changes in cation exchange capacity in intermittently waterlogged soil.
787 *Eur. Journ. Soil Sci.* **55**, 175-184.
788 Ganor J., Cama J., Metz, V. (2003) Surface protonation data of kaolinite-reevaluation based
789 on dissolution experiments. *J. Colloid Interface Sci.* **264**, 67-75.
790 Gin S., Jollivet P., Mestre J. P., Jullien M., Pozo C. (2001) French SON 68 nuclear glass
791 alteration mechanisms on contact with clay media. *Appl. Geochem.***16**, 861-881.
792 Gregg S. J. and Sing K. S. W. (1982) *Adsorption, Surface Area and Porosity* (ed. 2nd ed
793 Academic Press, London.
794 Guillaume D. (2002) Etude expérimentale du système fer-smectite en présence de solution à
795 80 °C et 300 °C. Ph. D. thesis, Université Henri Poincaré, Nancy I, spécialité Sciences
796 de l'Univers, 209 p.
797 Guillaume D., Neaman A., Cathelineau M., Mosser-Ruck R., Peiffert C., Abdelmoula M.,
798 Dubessy J., Villiéras F., Baronnet A., Michau N. (2003) Experimental synthesis of
799 chlorite from smectite at 300 °C in the presence of metallic Fe. *Clay Miner.* **38**, 281-
800 302.
801 Grillet Y., Rouquerol F., Rouquerol J. (1977) Etude de l'adsorption physique des gaz par une
802 procédure continue. I. Application à la détermination des surfaces spécifiques
803 d'adsorbants non poreux et mésoporeux. *J. Chem. Phys.* **74**, 179-182.
804 Habert B. (2000) Réactivité du fer dans les gels et les smectites. Ph. D. thesis, Université
805 Paris 6, spécialité Sciences des matériaux, 227 p.
806 Habert B., Jullien M., Kohler E., Bonnin D. (2006) Redox of iron in smectites. *Clay Science*
807 (in press).

808 Hillier S. and Velde B. (1992) Chlorite interstratified with a 7 Å mineral: an example from
809 offshore Norway and possible implications for the interpretations of the composition of
810 diagenetic chlorites. *Clay Miner*. **27**, 475-486.
811 Hillier S. (1994) Pore-lining chlorites in siliciclastic reservoir sandstones: electron
812 microprobe SEM and XRD data, and implications for their origin. *Clay Miner*. **29**, 665-
813 679.
814 Hochella M. F. Jr. (1995) Mineral surfaces: Their characterization and their chemical,
815 physical and reactive nature. In *Mineral surfaces* (eds. Vaughan D.J., Pattrick R.A.D.).
816 Chapman and Hall, London. pp. 17-60.
817 Hochella M. F. Jr., Rakovan J., Rosso K., Bickmore B., Rufe E. (1998) New directions in
818 mineral surface geochemical research using scanning probe microscopy. In *Mineral-*
819 *water interfacial reactions: Kinetics and mechanisms* (eds. Sparks D.L., Grundl T.J.).
820 ACS Symposium Series vol. **715**, American Chemical Society, Washington, D.C. pp.
821 37-56.
822 Hornibrook, E. R. C. and Longstaffe, L. J. (1996) Berthierine from the lower cretaceous
823 Clearwater formation, Alberta, Canada. *Clays Clay Miner*. **44**, 1, 1-21.
824 Huertas J. F., Chou L., Wollast R. (1999) Mechanism of kaolinite dissolution at room
825 temperature and pressure. Part II: Kinetic study. *Geochim. Cosmochim. Acta* **63**, 3261-
826 3275.
827 Kohler E. (2001) Réactivité des mélanges synthétiques smectite/kaolinite et
828 smectite/aluminium gel en présence d'un excès de fer métal. DRT report, Université
829 d'Evry Val d'Essonne, Evry, 101 p.
830 Lantenois S., Lanson B., Muller F., Bauer A., Jullien M. and Plançon A. (2005) Experimental
831 study of smectite interaction with metal iron at low temperature: 1. Smectite
832 destabilization. *Clays Clay Miner.* **53**, 597-612.

833 Latrille C., Jullien M., Pozo C. (2001) Element transfers in compacted clayey materials under
834 thermal gradient. Water-rock interaction Sardaigne, Cidu-Rosa editor, Swets &
835 Zeitlinger publisher, 1, 291-294.
836 Mamleev V. Sh., Villiéras F., Cases J. M. (2002) On the Use of Adsorption of Spherical
837 Molecules in Probing the Surface Topography: I. Patchwise Heterogeneity Model,
838 *Langmuir*, 2002, **18**, 2075-2088.
839 Mantin I. (1969) Mesure de la capacité d'échange des minéraux argileux par l'éthylène
840 diamine et les ions complexes de l'éthylène diamine. *Compte Rendu de l'Académie des*
841 *Sciences de Paris*, Série D, **269**, 815-818.
842 Marrochi Y., Razafitianamaharavo A., Michot L., Marty B. (2005) Low-pressure adsorption
843 of Ar, Kr, and Xe on carbonaceous materials (kerogen and carbon blacks), ferrihydrite,
844 and montmorillonite: Implications for the trapping of noble gases onto meteoritic
845 matter. *Geochim. Cosmochim. Acta*, **69**, 2419–2430.
846 McClellan A. L. and Harnsberger H. F. (1967) Cross sectional areas of molecules adsorbed
847 on solid surfaces. *J. Colloid Interfaces Sci*. **23**, 577-599.
848 Metz V., Raanan H., Pieper H., Bosbach D., Ganor J. (2005) Towards the establishment of a
849 reliable proxy for the reactive surface area of smectite. *Geochim. Cosmochim. Acta* **69**,
850 2581-2591.
851 Michot L., Francois M., Cases J. M. (1990) Surface heterogeneity studied by a quasi-
852 equilibrium gas adsorption procedure. *Langmuir* **6**, 677-681.
853 Michot L. J., Villiéras F., François M., Yvon J., LeDred R., Cases J.M. (1994) The structural
854 microscopic hydrophobicity of talc. *Langmuir* **10**, 3765-3773.
855 Michot L. J., Villiéras F., Lambert J. -F., Bergaoui L., Grillet Y., Robert J. -L. (1998) Surface
856 heterogeneity in micropores of pillared clays: the limits of classical pore-filling
857 mechanisms. *J. Phys.Chem*. **102**, 3466–3476.

Michot L. J., Villiéras F. (2002) Assessment of surface energetic heterogeneity of synthetic Na-Saponites. The role of layer charge. *Clay Miner.* **37**, 39-57.

Nagy K. L. (1994) Application of morphological data obtained using scanning force microscopy to quantification of fibrous illite growth rates. In *Scanning Probe Microscopy of Clay Minerals* (eds. Nagy K. L., Blum A. E.). Clay Minerals Society, pp. 204-239.

Nagy K. L., Blum A. E. (1994) Scanning probe microscopy of clay minerals, CMS Workshop Lectures vol. 7, Clay Minerals Society, Boulder, Colorado, 239 p.

Nagy K. L., Cygan R. T., Hanchar J. M., Sturchio N. C. (1999) Gibbsite growth kinetics on gibbsite, kaolinite and muscovite substrates: Atomic force microscopy evidence for epitaxy and an assessment of reactive surface area. *Geochim. Cosmochim. Acta* **63**, 2337-2351.

Neaman A., Pelletier M., Villiéras F. (2003) The effects of exchanged cations, compression and heating on textural properties of MX-80 bentonite and its corresponding purified montmorillonite. *Applied Clay Sci.*, **22**, 153-168.

Norrish K. (1954) The swelling of montmorillonite. *Discussions of the Faraday Society*, 18, 120-134.

Odin G. S. (1988) Green Marine Clays. In *Developments in sedimentology* (ed. Odin G.S.), 45. 446 p.

Odin G. S. (1990) Clay mineral formation at the continent-ocean boundary: the verdine facies. *Clay Miner.* **25**, 477-483

Olivier J. P. (1996) Calculating the size distribution of pore volume and area from adsorption isotherms: The application of deconvolution techniques to theories based on the Kelvin equation. Abstract book of 4th International Symposium on the characterization of Porous Solids, Bath, p L11.

Perronnet M. (2004) Réactivité des matériaux argileux dans un contexte de corrosion métallique. Application au stockage des déchets radioactifs en site argileux. Ph. D. thesis, Institut National Polytechnique de Lorraine, Nancy, discipline Géosciences, 280 p.

Rouquerol J., Rouquerol F., Grillet Y., Ward R. J. (1988) A critical assessment of quasi-equilibrium gas adsorption technique in volumetry, gravimetry and microcalorimetry. In *Characterization of porous solids* (eds. Hunger K.K.). Elsevier, Amsterdam, Oxford. pp. 67-76.

Sato T., Kuroda M., Yokoyama S., Fukushi K., Tanaka T., and Nakayama S. (2003) Mechanism and kinetics of smectite dissolution under alkaline conditions. *Geochim. Cosmochim. Acta* **67**, A415.

Sayed-Hassan M., Villiéras F., Razafitianamaharavo A., Michot L. J. (2005) Geometrical and energetic heterogeneity of kaolinites: The role of exchangeable cations on argon adsorption energy distribution, *Langmuir* **21**, 12283-12289.

Sayed-Hassan M., Villiéras F., Gaboriaud F., Razafitianamaharavo A. (2006) AFM and low-pressure argon adsorption analysis of geometrical properties of phyllosilicates. *J. Colloid Interface Sci.*, 296, 614-623.

Schlegel M. L., Manceau A., Chateigner D., Charlet L. (1999) Sorption of metal ions on clay minerals: I. Polarized EXAFS evidence for the adsorption of Co on the edges of hectorite particles. *J. Colloid Interface Sci.* **215**, 140-158.

Schwertmann U. (1979) Dissolution methods. In *Data Handbook for Clay Minerals and Other Non-metallic Minerals* (ed. H. Van Olphen and Fripiat J.J.). Pergamon Press. pp. 163-172

Sposito G. (1984) *The surface chemistry of soils*. Oxford University Press, New York, 227 p.

907 Sutheimer S. H., Maurice P. A., Zhou Q. (1999) Dissolution of well and poorly crystallized
908 kaolinites: Al speciation and effects of surface characteristics. *Am. Mineral.* **84**, 620-
909 628.
910 Stucki J. W., Golden D. C., Roth C. B. (1984) Effects of reduction and reoxidation of
911 structural iron on the surface charge and dissolution of dioctahedral smectites. Clays
912 Clay Miner, **32**, 350-356.
913 Tournassat C., Neeman A., Villiéras F., Bosbach D., Charlet L. (2003) Nanomorphology of
914 montmorillonite particles: estimation of the clay edge sorption site density by low-
915 pressure gas adsorption and AFM observations. *Am. Mineral.* **88**, 1989-1995.
916 Villiéras F., Cases J. -M., François M., Michot L. J. and Thomas F. (1992) Textural
917 properties and surface energetic heterogeneity of solids from modeling of low pressure
918 gas adsorption isotherms. *Langmuir* **8,** 1789-1795.
919 Villiéras F., Michot L. J., Bardot F., Cases J. M., François M., Rudzinski W. (1997a) An
920 improved derivative isotherm summation method to study surface heterogeneity of clay
921 minerals. *Langmuir* **13**, 1104-1117.
922 Villiéras F., Michot L. J., Cases J M., Berend I., Bardot F., François M., Gérard G., Yvon J.
923 (1997b) Static and dynamic studies of the energetic surface heterogeneity of clay
924 minerals. In *Equilibria and dynamics of gas adsorption on heterogeneous solid*
925 *surfaces, Studies in surface science and catalysis,* ***104*** (eds. Rudzinski W., Steele W.
926 A., Zgrablich G.,). Elsevier Science Publication B.V., Amsterdam. pp. 573-623.
927 Villiéras F., Michot L. J., Bernardy E., Chamerois M., Legens C., Gérard G., and Cases J. M.
928 (1999) Assessment of surface heterogeneity of calcite and apatite: from high resolution
929 gas adsorption to solid-liquid interface, *Colloid Surface A* **146**, 163-174.

930 Villiéras F., Michot L. J., Bardot F., Chamerois M., Eypert-Blaison C., François M., Gérard
931 G., Cases J. M. (2002) Surface heterogeneity of minerals. *Compte Rendu Geosciences*
932 **334**, 597-609.
933 Villiéras F., Chamerois M., Bardot F., Michot L. J. (2002) Evaluation of wetting properties of
934 powders from gas adsorption experiments. In *Contact Angle, Wettability and Adhesion*,
935 Volume 2, (ed. Mittal K.L.). VSP, Utrecht. pp. 435-447.
936 Walker J. R., Thompson G. R. (1990) Structural variations in illite and chlorite in a
937 diagenetic sequence from the Imperial Valley, California. *Clays Clay Miner*. **38**, 315-
938 321.
939 White G. N. and Zelazny L. W. (1988) Analysis and implications of the edge structure of
940 dioctahedral phyllosilicates. *Clays Clay Miner.* **36**, 141-146.
941 Wilson J., Cressey G., Cressey B., Cuadros J., Ragnarsdottir K. V., Savage D., Shibata
942 M.(2006) The effect of iron on montmorillonite stability. (II) Experimental
943 investigation. *Geochim. Cosmochim. Acta*, **70**, 323-336
944 Zachara J. M. and McKinley J. P. (1993) Influence of hydrolysis on the sorption of metal
945 cations by smectites: Importance of edge coordination reactions. *Aquat. Sci.* **55**, 250-
946 261.
947 Zega T. Z. and Buseck P. R. (2003) Fine-grained rim mineralogy of the Cold BoKKeveld
948 CM Chondrite. *Geochim. Cosmochim. Acta*, **67**, 1711-1721.
949 Zolensky M. E. and McSween H. Y. (1988) Aqueous alteration. In *Meteorites and the early*
950 *solar system* (eds. Kerridge J.F. and Matthews M.S). University of Arizona Press,
951 Tucson. pp. 114-143.

8. TABLES

Table 1. Mineralization (in $mg.L^{-1}$) of Evian natural mineral water (Evian).

	CO_3^{2-}	Ca^{2+}	Mg^{2+}	SiO_2	SO_4^{2-}	Na^+	Cl^-	NO_3^-	K^+
$mg.L^{-1}$	357	78	24	13.5	10	5	4.5	3.8	1

Table 2. pH evolution for the tests at 80°C during 3 months.

	I/C=0	I/C=1/3
OrduArtikli	8.5	8.7
Nontronite	7.7	8.4
Prassa	8.0	10.6

Table 3. Numerical results derived from BET, t-plot and mesoporosity analyses of the experimental adsorption/desorption isotherms found in Figure 8. BET information was obtained in the 0.05-0.15 P/Po range, t-plot information was obtained from the 0.02-0.22 P/Po range and mesoporosity information was calculated from the adsorption branch using parallel shaped mesopores. Vm: monolayer volume (STP gas cm^3/g); C: BET energy constant; Stot: total specific surface area (+/- $4m^2/g$); Sμpores: equivalent specific surface area of micropores (+/- 20%); Sext: external specific surface area (= Stot-Sμpores, +/- 20%), Vmeso: total volume of mesopores (geometrical volumes, considering that liquid nitrogen density is 0.808) and S_{Ar}, Argon specific surface area derived from the modeling of the low pressure argon adsorption isotherm (see next section and Table 4).

	BET			t-plot			Mesoporosity		DIS
	Vm	C	Stot	Sμpores	Sext	Stot	Stot	Vmeso	S_{Ar}
	cm^3/g		m^2/g	m^2/g	m^2/g	m^2/g	m^2/g	cm^3/g	m^2/g
Orduartikli	23.2	360	101	26	80	107	109	0.0088	81
Nontronite	24.7	324	108	26	86	112	115	0.0125	78
Prassa	23.4	154	102	6	97	103	103	0.0242	93

970 Table 4. Main parameters obtained from the application of the DIS method to Ar adsorption
971 at 77 K on the studied montmorillonites.

	ΔG/RT =- ln(P/Po)	ω/kT	Vm cm^3/g	SSA m^2/g
		Orduartikli Na		
1	11.9	0.5	1.2	4.5
2	9.6	1.5	0.4	1.6
3	7.1	0.5	6.4	23.7
4	4.6	1.3	11.6	43.2
5	2.8	2.2	2.2	8.1
			Total	81.1
		Nontronite Na		
1	12.6	0.9	0.7	2.8
2	9.9	0.3	1.2	4.4
3	6.8	0.2	5.4	20.0
4	4.5	1.5	10.6	39.4
5	2.8	2.0	2.9	10.9
			Total	77.5
		Prassa Na		
1	12.8	0.7	0.5	1.8
2	10.2	0.2	0.8	2.9
3	6.6	-0.3	5.5	20.3
4	4.6	1.4	13.1	48.6
5	2.5	2.0	5.1	18.9
			Total	92.5

972

973 Table 5. Geometrical characteristics of the dry particles of the three Na-exchanged purified
974 smectites.

	OrduArtikli	Nontronite	Prassa
Basal surface area (m^2/g)	51.2	50.3	67.5
Edge surface area (m^2/g)	29.8	27.2	25.0
l (nm)	50	54	59
t (nm)	14	15	11
Particle volume (nm^3)	35000	43740	38291

975

9. FIGURES

Figure 1. CEC evolution for the tests at 80°C during 3 months, I/C=0.

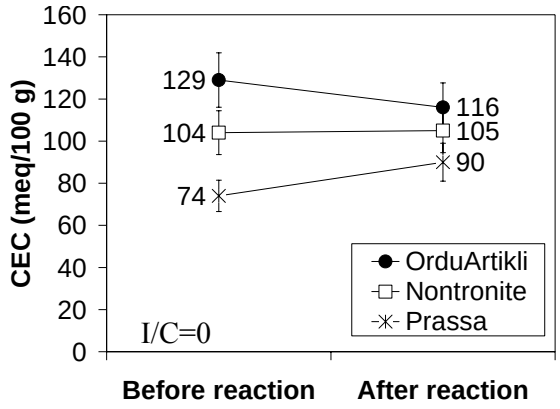

Figure 2. CEC evolution for the tests at 80°C during 3 months, I/C=1/3.

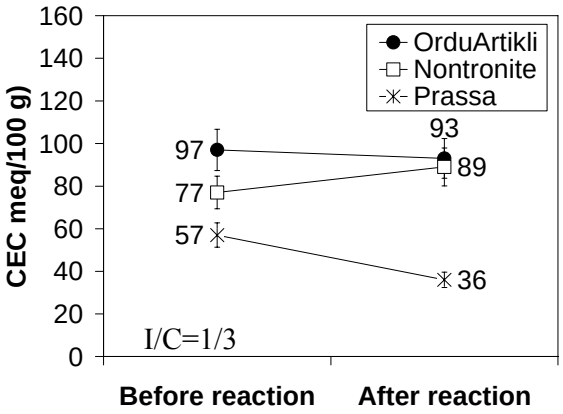

Figure 3. Evolution of the distribution of iron components in the "Nontronite-Fe(0) mixture" (I/C=1/3) throughout the reaction (80°C – 3 months). Obtained using ^{57}Fe Mössbauer quantification.

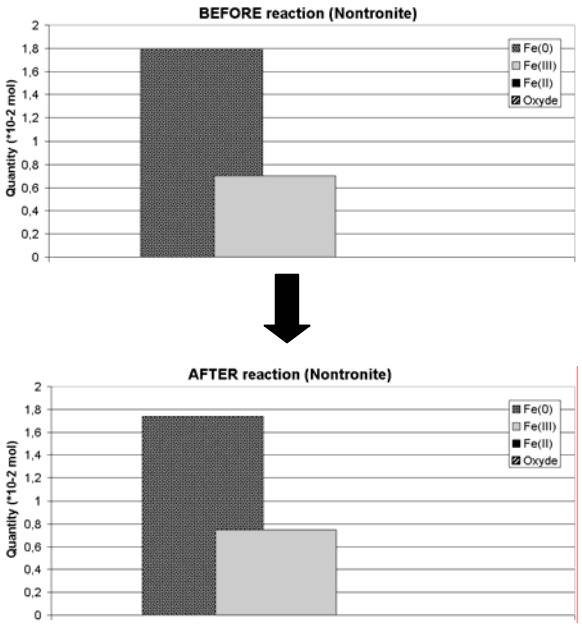

Figure 4. Evolution of the distribution of iron components in the "Prassa-Fe(0) mixture" (I/C=1/3) throughout the reaction (80°C – 3 months). Obtained using ^{57}Fe Mössbauer quantification.

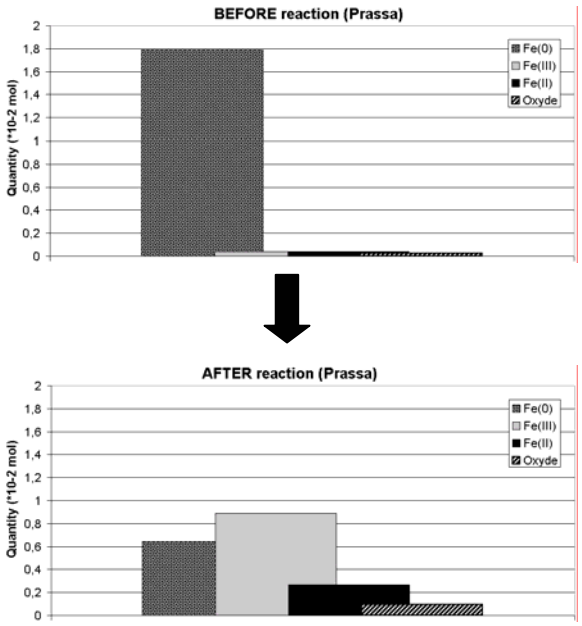

997 Figure 5. X-Ray diffractograms of the OrduArtikli-Fe(0) mixture before and after reaction at

998 80°C for a duration of 3 months, I/C=1/3.

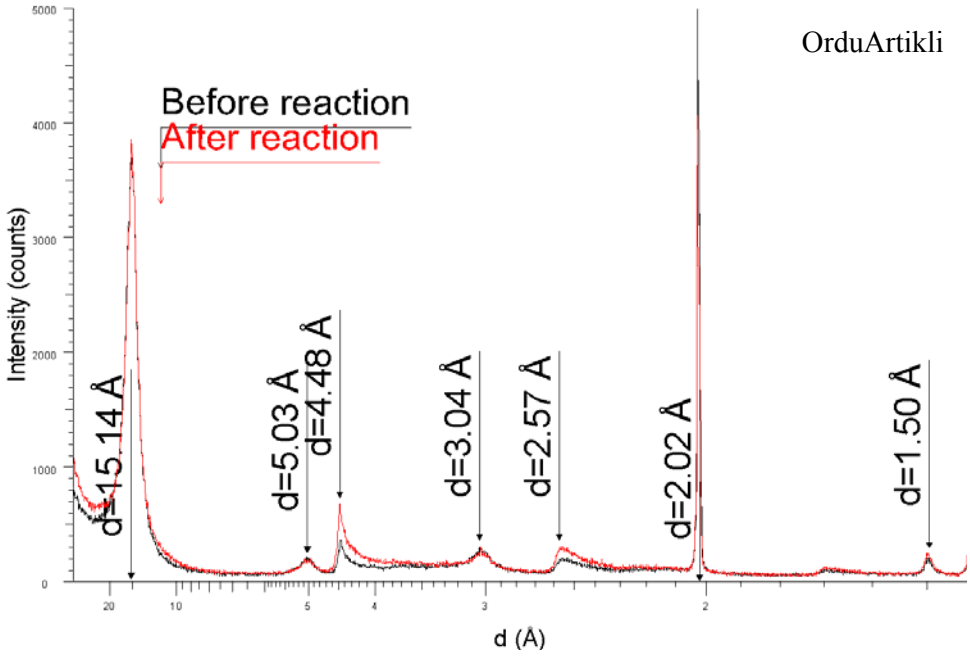

999

1000

1001 Figure 6. X-Ray diffractograms of the Nontronite-Fe(0) mixture before and after reaction at

1002 80°C for 3 months, I/C=1/3.

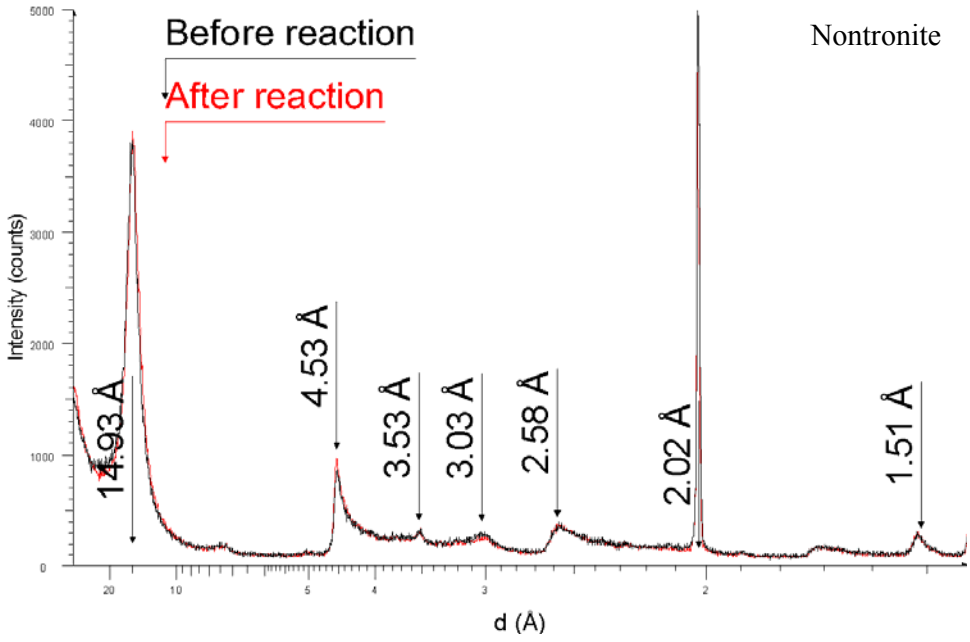

1003

1004

1005 Figure 7. X-Ray diffractograms of the Prassa-Fe(0) mixture before and after reaction at 80°C

1006 for 3 months, I/C=1/3.

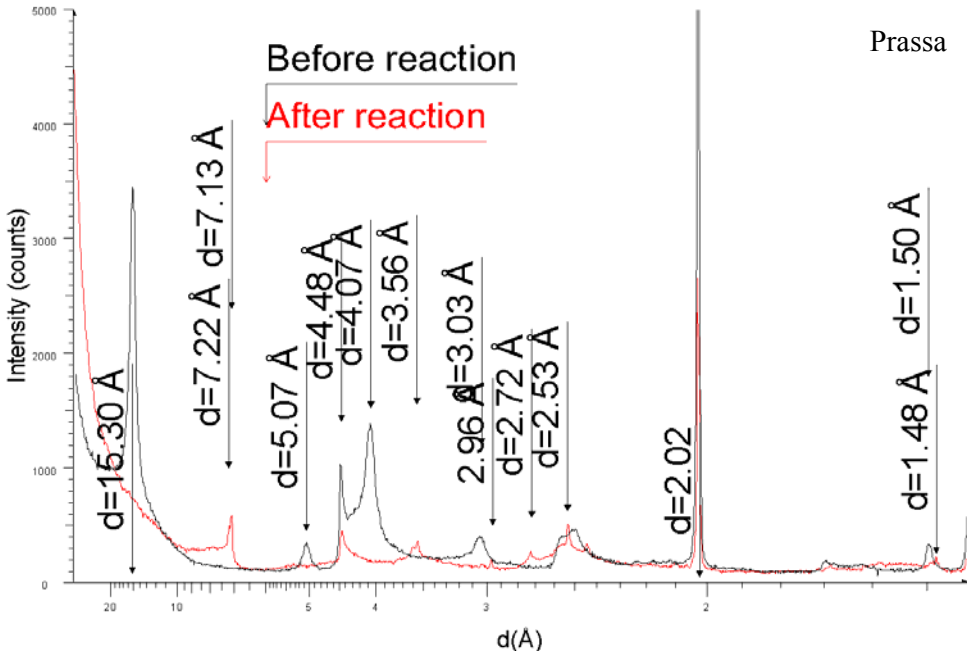

1007

1008

1009 Figure 8. Nitrogen adsorption/desorption isotherms at 77 K

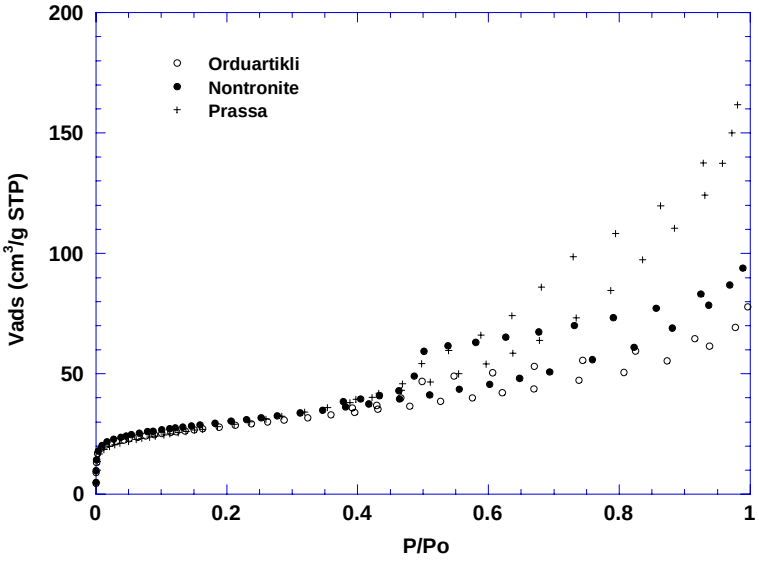

1010

1011 Figure 9. Pore size distributions calculated form nitrogen adsorption/desorption isotherms of
1012 Figure 8. Plain lines: adsorption Pore Size Distribution (true PSD); dotted line: desorption
1013 Pore Size Distribution (access PSD).

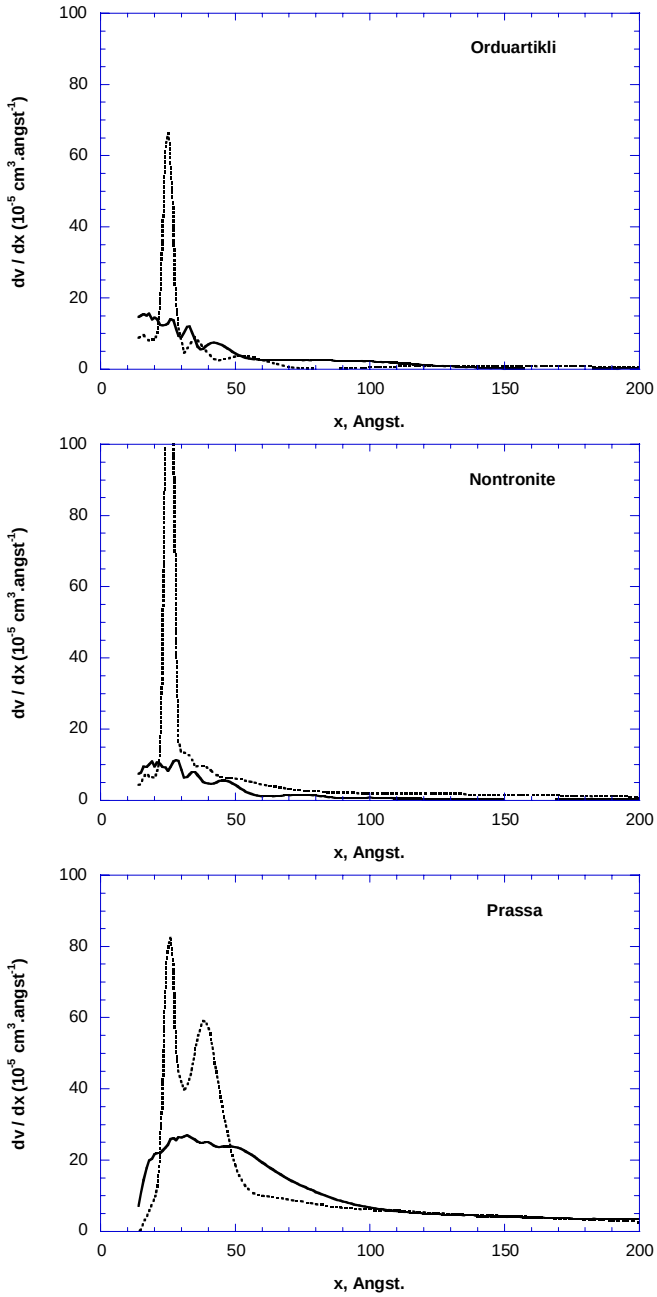

1014

1015 Figure 10. Low pressure argon adsorption isotherms at 77 K

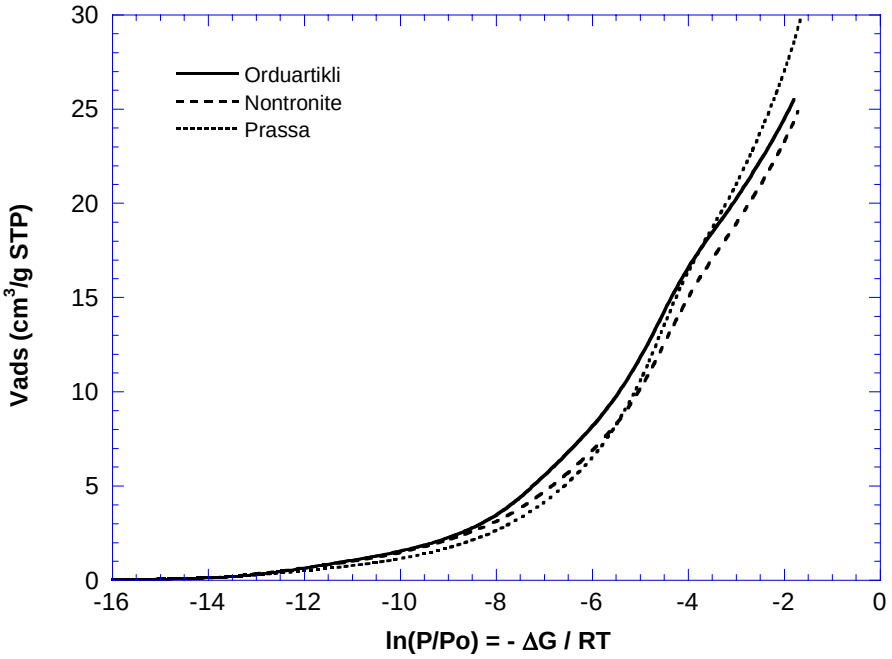

1016

Figure 11. Adsorption energy distributions (plain lines) derived from low pressure argon adsorption at 77 K and local isotherms (Bragg-William-Temkin models, dotted lines), used to model experimental curves. Multilayer contribution in the low energy region (right hand side of the curves) was mathematically removed before the DIS fitting procedure (Villiéras et al., 1997a; Mamleev et al., 2002). Fitting parameters are collected in Table 4.